

Materials Contrast in Piezoresponse Force Microscopy

Sergei V. Kalinin,*

Condensed Matter Sciences Division, Oak Ridge National Laboratory, Oak Ridge, TN 37831

Eugene A. Eliseev

Institute for Problems of Materials Science, National Academy of Science of Ukraine,
3, Krjjanovskogo, 03142 Kiev, Ukraine

Anna N. Morozovska[†]

V. Lashkaryov Institute of Semiconductor Physics, National Academy of Science of Ukraine,
41, pr. Nauki, 03028 Kiev, Ukraine

Abstract

Piezoresponse Force Microscopy contrast in transversally isotropic material corresponding to the case of c^+ - c^- domains in tetragonal ferroelectrics is analyzed using Green's function theory by Felten et al. [J. Appl. Phys. 96, 563 (2004)]. A simplified expression for PFM signal as a linear combination of relevant piezoelectric constant are obtained. This analysis is extended to piezoelectric material of arbitrary symmetry with weak elastic and dielectric anisotropies. This analysis provides a framework for interpretation of PFM signals for systems with unknown or poorly known local elastic and dielectric properties, including nanocrystalline materials, ferroelectric polymers, and biopolymers.

PACS: 77.80.Fm, 77.65.-j, 68.37.-d

* Corresponding author, sergei2@ornl.gov

[†] Corresponding author, morozo@i.com.ua

In the last decade, Piezoresponse Force Microscopy (PFM) has become the primary tool for the characterization of ferroelectric and piezoelectric materials on the nanoscale.^{1,2,3,4,5} The ability to image ferroelectric domain structure with nanometer resolution, relative insensitivity to topographic cross-talk, and capability to probe local switching behavior have resulted in strong interest to quantitative interpretation of PFM signal in terms of relevant material properties. In general, calculation of the electromechanical response induced by the biased tip requires the solution of coupled electromechanical problem, currently available only for uniform transversally isotropic case.^{6,7} This solution is also limited to the strong indentation case, in which the fields generated outside the contact area are neglected. An alternative approach for calculation of electromechanical response is based on the decoupling approximation. In this case, electric field in the material is calculated using rigid electrostatic model (no piezoelectric coupling), the strain or stress field is calculated using constitutive relations for piezoelectric material, and the displacement field is evaluated using appropriate Green's function for isotropic or anisotropic solid. The 1D version of this model was originally suggested by Ganpule *et al.*⁸ to account for the effect of 90° domain walls on PFM image. The electrostatic field was calculated using complete 3D model. Completely 1D approach was adapted by Agronin *et al.*⁹ to yield closed-form solutions for PFM signal. Decoupling approach was extended to 3D by Felten *et al.*¹⁰ using analytical form for corresponding Green's function. Independently, Scrymgeour and Gopalan¹¹ have used finite element method to calculate the PFM signals across the domain walls. The advantage of the decoupled 3D models is that PFM signal can be determined for arbitrary electric fields and PFM response can be calculated for various microstructural elements such as domain walls. However, existing solutions are extremely cumbersome and require numerical calculations.

Here, we analyze PFM contrast in transversally isotropic material corresponding to the case of $c^+ - c^-$ domains in tetragonal ferroelectrics using Green's function theory by Felten *et al.*¹⁰ The closed-form expressions for PFM signal, including relative contributions of individual elements of piezoelectric constant tensor, elastic properties, and effects of dielectric anisotropy of material on PFM signal, are derived. The approximate expression for vertical and lateral PFM signal for anisotropic piezoelectric with weak elastic and dielectric anisotropies is obtained.

The Green's function approach is based on (1) calculation of the electric field for rigid dielectric ($d_{ijk} = e_{ijk} = 0$), (2) calculation of stress field $X_{ij} = e_{kij} E_k$ in piezoelectric material and (3) calculation of the mechanical displacement field using Green's function for non-piezoelectric elastic body. This approach, while not being rigorous, significantly simplifies the problem and in

particular allows the effective symmetries of elastic, dielectric, and piezoelectric properties of material to be varied independently. Shown in Fig. 1 are crystallographic orientation dependence for effective dielectric, piezoelectric, and elastic properties for BaTiO_3 and LiNbO_3 .¹² In particular, we note that dielectric and particularly elastic properties described by positively defined second- and fourth rank tensors are necessarily more isotropic than piezoelectric properties described by third-rank tensor. Hence, in many cases elastic and dielectric properties can be approximated as isotropic.

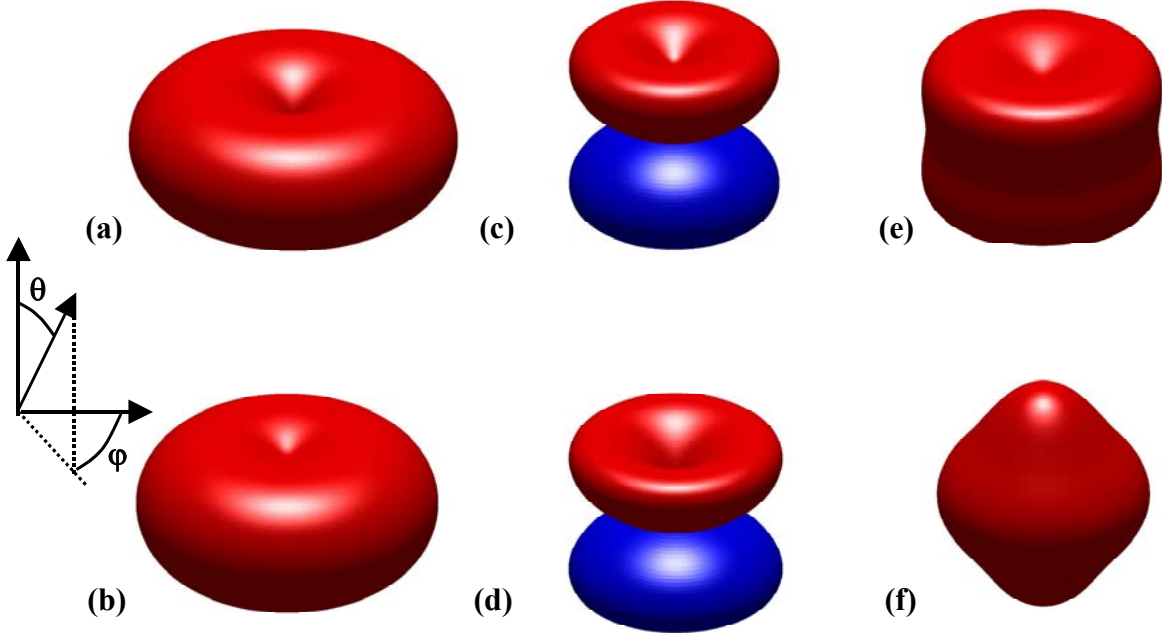


Fig. 1. Crystallographic orientation dependence of effective dielectric constant in z-direction (a,b), effective longitudinal piezoelectric constant (c,d) and effective Young's modulus (e,f) for BaTiO_3 (a,c,e) and LiNbO_3 (b,d,f).

For transversally isotropic material, the tip-induced electric field can be determined using simple image charge models. For spherical part of the tip apex, the solution is rigorous, while for the conical part of the tip an approximate line-charge model can be used.^{13,14} Here, we develop the solution for single charge above the ferroelectric surface, and later develop the unified theory for arbitrary point charge distribution.

The potential in the transversally isotropic dielectric material produced by the point charge, Q , at the distance, d , above the surface, is

$$V_i(\rho, z) = \frac{Q}{2\pi\epsilon_0(\kappa+1)} \frac{1}{\sqrt{\rho^2 + (z/\gamma + d)^2}}, \quad (1)$$

where ρ and z are radial and vertical coordinate, $\kappa = \sqrt{\epsilon_{33}\epsilon_{11}}$ is effective dielectric constant, and $\gamma = \sqrt{\epsilon_{33}/\epsilon_{11}}$ is dielectric anisotropy factor [Fig. 2(a)].

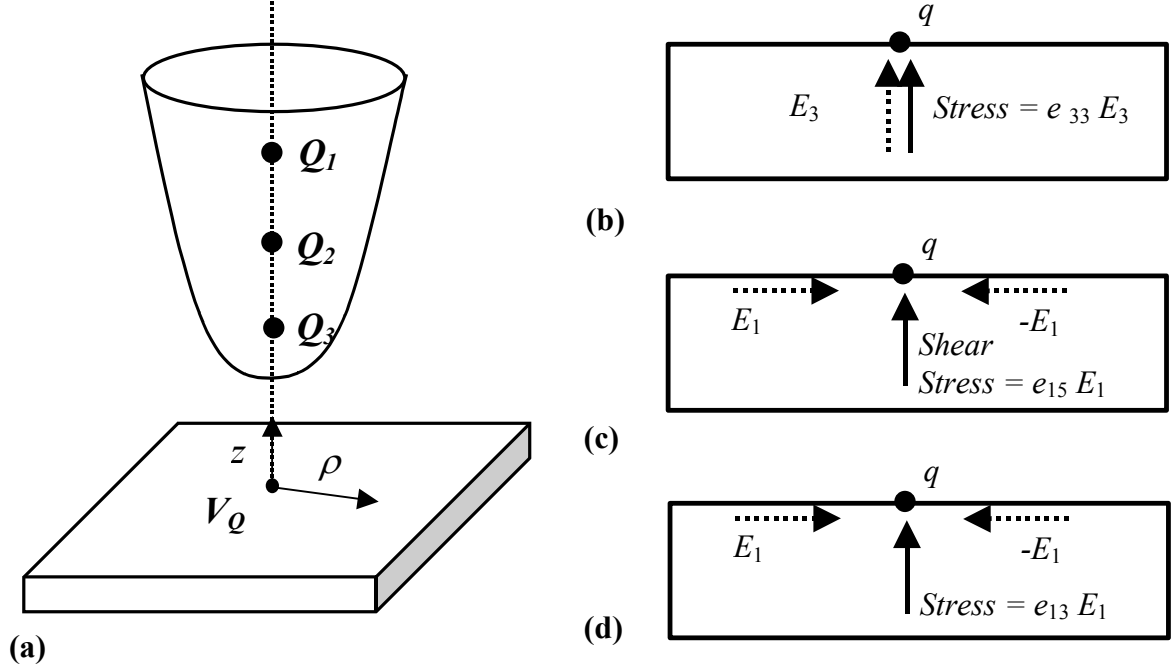


Fig. 2. (a) Tip representation using image charge distribution in the PFM experiment. Schematics of contributions of (b) e_{33} , (c) e_{15} and (d) e_{31} to the PFM signal.

The displacement field can be calculated using Green's function approach suggested by Felten et al.¹⁰ The displacement vector $u_i(\mathbf{x})$ at position \mathbf{x} is

$$u_i(\mathbf{x}) = \int_{x_3=0}^{\infty} \int_{x_2=-\infty}^{\infty} \int_{x_1=-\infty}^{\infty} e_{kl} E_k(\mathbf{x}') \frac{\partial}{\partial x'_l} G_{ij}(\mathbf{x}, \mathbf{x}') d\mathbf{x}' \quad (2)$$

where \mathbf{x}' is the coordinate system related to the material, e_{kl} are the piezoelectric coefficients ($e_{kij} = d_{klm} c_{lmij}$) and the Einstein summation convention is used. $E_k(\mathbf{x}')$ is the electric field produced by the probe. For most ferroelectric perovskites, the symmetry of the elastic properties can be approximated as cubic (anisotropy of elastic properties is much smaller than of dielectric and piezoelectric properties) and therefore isotropic approximation is used. The Green's function for isotropic semi-infinite half-plane is:¹⁵

$$G_{ij}(\mathbf{x}, \mathbf{x}') = \frac{1+\nu}{2\pi Y} \left[\frac{\delta_{ij}}{R} + \frac{(x_i - x'_i)(x_j - x'_j)}{R^3} + \frac{1-2\nu}{R+x'_3} \left(\delta_{ij} - \frac{(x_i - x'_i)(x_j - x'_j)}{R(R+x'_3)} \right) \right] \quad (3)$$

where $R = \sqrt{(\mathbf{x} - \mathbf{x}')^2}$, Y is Young's modulus and ν is Poisson ratio. After lengthy manipulations, the Eq. (3) is integrated analytically to yield the transverse displacement of the surface ($z = 0$) at the position of the tip, i.e. vertical PFM signal, as

$$u_3(\rho) = \frac{Q}{2\pi\epsilon_0} \frac{1+\nu}{Y} \frac{1}{\sqrt{\rho^2 + d^2}} (e_{31}f_1(\gamma) + e_{15}f_2(\gamma) + e_{33}f_3(\gamma)), \quad (4)$$

and $u_1(0) = u_2(0) = 0$. Hereinafter we use $e_{31} \equiv e_{311}$, $e_{33} \equiv e_{333}$, $e_{15} \equiv e_{113}$ in Voigt representation when possible. The functions $f_i(\gamma)$ that determine contributions of piezoelectric constants e_{in} to the overall signal depend only on the dielectric anisotropy of the material, γ , as

$$f_1 = \frac{\gamma}{(1+\gamma)^2} + (1-2\nu) \left(1 - 2\gamma + 2\gamma^2 \ln\left(1 + \frac{1}{\gamma}\right) - \frac{1}{(1+\gamma)} \right) \quad (5)$$

$$f_2 = - \left(\frac{2\gamma^2}{(1+\gamma)^2} + (1-2\nu) \left(\frac{4\gamma + 5\gamma^2 + 3\gamma^3 + 6\gamma^4}{2(1+\gamma)} + 3\gamma^2(1+\gamma^2) \ln\left(\frac{\gamma}{\gamma+1}\right) \right) \right) \quad (6)$$

$$f_3 = - \frac{\gamma}{(1+\gamma)^2} + (1-2\nu) \left(\frac{-1 + 3\gamma + 6\gamma^2}{2(1+\gamma)} - (1+3\gamma^2) \ln\left(1 + \frac{1}{\gamma}\right) \right) \quad (7)$$

The contributions of different piezoelectric constants to the overall displacement are shown schematically in Fig. 2. Normal component of electric field is related to the vertical stress component by piezoelectric constant e_{33} , as shown in Fig. 2 (b). The second contribution to response originates from the lateral component of electric fields related to the shear stress component by piezoelectric constant e_{15} as shown in Fig. 2 (c). Finally, the constant e_{31} relates the stress in z-direction to the normal field component, as shown in Fig. 2 (d).

Shown in Fig. 3 (a,b) are functions $f_i(\gamma)$ that determine contributions of piezoelectric constants e_{nm} to the overall signal. For most of ferroelectric oxides $\gamma \approx 0.3 - 1$, while $\gamma \approx 10.5$, and 2.3 for Rochelle salt and triglycine sulfate respectively. The function $f_3(\gamma)$ rapidly decays with γ , indicating the decreasing contribution of e_{33} to signal. The signal decreases for low compressibility materials (high ν). Conversely, $f_2(\gamma)$ that determines contribution of constant e_{15} to signal increases with γ . Finally, $f_1(\gamma)$ has a maximum and is much smaller than $f_3(\gamma)$, $f_2(\gamma)$.

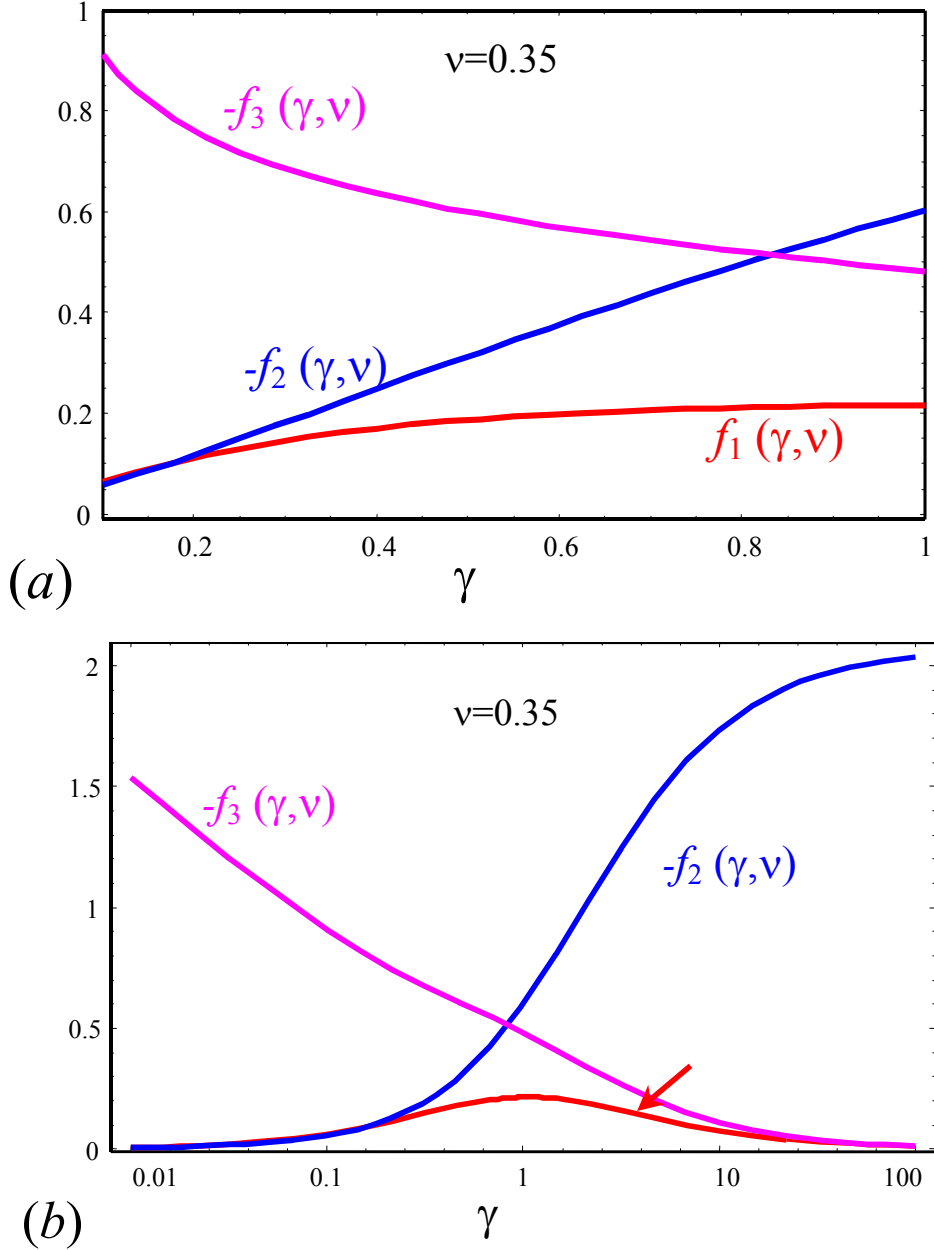


Fig. 3. (a) Plot of functions $f_i(\gamma, \nu)$ for $\nu = 0.35$ in the $(0,1)$ interval corresponding to most ferroelectric oxides. (b) Plot in the logarithmic scale in the $(10^{-2}, 10^2)$ interval illustrating the asymptotic behavior of the dissimilar contributions with dielectric anisotropy.

To calculate the PFM signal, we note the similarity between Eq. (4) and Eq. (1) for $z = 0$.

Hence, we obtain

$$u_3(0) = V_Q \frac{1+\nu}{Y} (e_{31}f_1(\gamma) + e_{15}f_2(\gamma) + e_{33}f_3(\gamma)), \quad (8)$$

where $V_Q = V_i(\rho, z = 0)$. Thus, the PFM response is proportional to the potential on the surface induced by the charge. This is also true for the several charges located on the same line along the surface normal, i.e. for sphere and approximate line charge approximations for the tip. In all these case, the response depends only on the maximal surface potential induced by the tip, and does not depend on exact charge distribution, in agreement with previous results.¹³

The electromechanical responses calculated using Eq. (8) and exact theory⁶ are shown in Table 1. In the first column, compared are the elastic modulus $C_1^*/2\pi$ and Young's modulus in the z-direction $1/s_{33}$.¹²

Table 1. Materials Properties and Calculated Responses

Material	Elastic constants [GPa]		Dielectric anisotropy γ	Piezoelectric properties [pm/V]		Approximate solution [pm/V]		
	$C_1^*/2\pi$	$1/s_{33}$		d_{33}	C_3^*/C_1^*	d_{33}^*	$d_{33}^*(\gamma = 1)$	$d_{33}^*(d)$
BaTiO ₃	128.3	63.67	0.24	85.59	38.2	63.6	159.6	106.2
LiNbO ₃	205.95	202.55	0.6	6.31	11.63	14.0	18.7	17.0
LiTaO ₃	248.3	228.1	0.94	8.328	11.28	13.2	13.5	13.7
PZT6B	114.5	107.2	0.98	74.94	71.11	78.3	78.6	88.3

Note good agreement between these values for all materials excluding BaTiO₃, in which the anisotropy of mechanical properties is significant. In the second column, listed are coefficients of dielectric anisotropy. In the third column, compared are the values of piezoelectric constant, d_{33} , and electromechanical response from exact theory, C_3^*/C_1^* . Finally, in the last column we tabulate the values of electromechanical response $d_{33}^* = u_3(0)/V_Q$ calculated from Eq. (8) for $Y = C_1^*/2\pi$ and $\nu = 0.35$, electromechanical response for zero dielectric anisotropy $d_{33}^*(\gamma = 1)$, and electromechanical response, $d_{33}^*(d)$, calculated for the values of $e_{im} = d_{in}c_{nm}$, where material is assumed to be elastically isotropic. In this latter case when strain piezoelectric constants d_{in} are used, the response is independent on Young's modulus and is determined only by the Poisson ratio of the material.¹⁰ Note that for materials with weak ($\gamma \approx 1$) and moderate ($\gamma \approx 0.6$) dielectric anisotropies the approximate PFM response from Eq. (8) is in a very good agreement with exact result, validating the use of this model. The relative analysis of different contributions in Eq. (8) suggests that the response is dominated by e_{33} and e_{35} terms, while e_{13} provides only

minor contribution (e.g. for BTO relative contributions of (e_{31}, e_{33}, e_{15}) are $(0.06, 44, 50)$, for LiNbO_3 $(0.01, 35, 64)$, and for PZT 6B $(0.03, 54, 43)$).

From data in Table I, certain material can be approximated as both elastically and dielectrically isotropic. Here we extend Eq. (8) to the fully anisotropic piezoelectric solids with weak dielectric anisotropy ($\epsilon_{ij} \approx \delta_{ij} \kappa \epsilon_0$). In this case, after lengthy integrations (see Appendix A) the components of surface displacement related to vertical and lateral PFM signals^{16,17} are found from Eqs. (1,2,3) as $u_i(\mathbf{x}) = e_{klj} U_{klj}(\mathbf{x})$, where tensor $U_{klj}(0)$ is symmetrical on the transposition of the indexes i, j and k, l . Using Voigt matrix notation, $U_{klj}(0)$ can be represented as

$$\hat{U}(0) = V_Q \frac{1+\nu}{Y} \begin{pmatrix} a_{11} & a_{12} & a_{13} & 0 & 0 & 0 \\ a_{12} & a_{11} & a_{13} & 0 & 0 & 0 \\ a_{31} & a_{31} & a_{33} & 0 & 0 & 0 \\ 0 & 0 & 0 & a_{44} & 0 & 0 \\ 0 & 0 & 0 & 0 & a_{44} & 0 \\ 0 & 0 & 0 & 0 & 0 & a_{66} \end{pmatrix}, \quad (9)$$

where $a_{11} = -0.406 + 0.375\nu$, $a_{12} = -0.469 + 0.125\nu$, $a_{13} = -0.489 + 0.227\nu$, $a_{31} = -1.125 + 0.5\nu$, $a_{33} = -1.023 + 1.545\nu$, $a_{44} = 0.0681 + 0.114\nu$, $a_{66} = 0.0313 + 0.125\nu$.¹⁸

Thus, Eq. (9) provides approximate description of PFM response for the material of arbitrary symmetry and crystallographic orientation. The detailed analysis of PFM contrast in the anisotropic case is reported elsewhere.¹⁹

To summarize, a simplified expressions for PFM signal as a linear combination of relevant piezoelectric constant are obtained for transversally isotropic dielectric medium for weak elastic anisotropy. The solution can be readily extended for arbitrary tip model. For sphere-plane and line charge models when the image charges are located on the tip axis of symmetry, the response is proportional to the potential induced by the tip on the surface and is independent on exact image charge distribution in the tip. This analysis is extended to piezoelectric material of arbitrary symmetry with weak elastic and dielectric anisotropies. The calculated response is dependent on either (a) the piezoelectric strain constants, e_{ijk} , of the materials and elastic properties (Y, ν) that can be determined from the indentation experiments or (b) piezoelectric stress constants, d_{ijk} , and Poisson modulus, ν , only, thus providing a framework for

interpretation of PFM signals for systems with unknown or poorly known local elastic properties, including nanoferroelectrics, ferroelectric polymers, and biopolymers.

Research supported by Oak Ridge National Laboratory, managed by UT-Battelle, LLC, for the U.S. Department of Energy under Contract DE-AC05-00OR22725.

APPENDIX A. Exact analytical solution for the initial and final states response in piezoelectrically anisotropic media

The displacement vector $u_i(\mathbf{x})$ caused by AFM tip electric field is given by equation

$$u_i(\mathbf{x}) = e_{klj} U_{klj}(\mathbf{x}) \quad (\text{A.1})$$

Hereinafter e_{klj} is piezoelectric tensor. The components of tensor $U_{klj}(\mathbf{x})$ are the following convolution

$$U_{klj}(\mathbf{x}) = \int_{x_3=0}^{\infty} \int_{x_2=-\infty}^{\infty} \int_{x_1=-\infty}^{\infty} E_k(\mathbf{x}') \frac{\partial G_{ij}(\mathbf{x}, \mathbf{x}')}{\partial x'_l} d\mathbf{x}' . \quad (\text{A.2})$$

$U_{klj}(\mathbf{x})$ is symmetrical only on the indexes i and j transposition and thus has 54 nontrivial components in general case. Integration by parts in Eq. (A.2) allows one to rewrite them as follows

$$U_{klj}(\mathbf{x}) = -J_{klj}(\mathbf{x}) - \delta_{l3} A_{kij}(\mathbf{x}) . \quad (\text{A.3})$$

Here δ_{l3} is delta-Kroneker symbol and

$$J_{klj}(\mathbf{x}) = \int_{x_3=0}^{\infty} \int_{x_2=-\infty}^{\infty} \int_{x_1=-\infty}^{\infty} \frac{\partial E_k(\mathbf{x}')}{\partial x'_l} G_{ij}(\mathbf{x}, \mathbf{x}') d\mathbf{x}' \quad (\text{A.4})$$

$$A_{kij}(x_1, x_2, x_3) = \int_{x_2=-\infty}^{\infty} \int_{x_1=-\infty}^{\infty} E_k(x'_1, x'_2, x'_3 = 0) G_{ij}(x'_1 - x_1, x'_2 - x_2, x'_3 = 0, x_3) dx'_1 dx'_2 \quad (\text{A.5})$$

In order to obtain exact analytical solution all further integrations are carried out for $x_3 = 0$ and $\gamma = 1$ for the sake of simplicity (see details in Appendix B). Also the usual designations $x_1 = x$, $x_2 = y$ and $\rho^2 = x^2 + y^2$ are introduced for clearness.

We derived the following **rules**.

1) A threefold integral $J_{klj}(\mathbf{x})$ is symmetrical on the transposition of indexes in the pairs $\{i, j\}$ and $\{k, l\}$ respectively (since $\partial E_k(\mathbf{x}')/\partial x'_l \equiv \partial E_l(\mathbf{x}')/\partial x'_k$ and $G_{ij}(\mathbf{x}, \mathbf{x}') \equiv G_{ji}(\mathbf{x}, \mathbf{x}')$):

$$J_{klj}(\mathbf{x}) = J_{klji}(\mathbf{x}) = J_{lkji}(\mathbf{x}) = J_{lkij}(\mathbf{x})$$

2) Unknown integrals $J_{klji}(x)$ that contains indexes “1” or/and “2” can be obtained from the already calculated ones by simultaneous permutation of indexes “1” \leftrightarrow “2” and coordinates $x \leftrightarrow y$, e.g.: $J_{1222}(x,y) \equiv J_{1211}(y,x)$, $J_{1223}(x,y) \equiv J_{2113}(y,x)$, $J_{2211}(x,y) \equiv J_{1122}(y,x)$, $J_{2311}(x,y) \equiv J_{1322}(y,x)$, $J_{2333}(x,y) \equiv J_{1333}(y,x)$.

3) Since the electric field E_k satisfies the equation $\partial E_k(x')/\partial x'_k \equiv 0$ inside the piezoelectric material (Coulomb law in differential form $\text{div}E = 0$) the integrals $J_{33ij}(x,y)$ can be expressed through $J_{11ij}(x,y)$ and $J_{22ij}(x,y)$ in the following way:

$$J_{33ij}(x,y) \equiv -J_{11ij}(x,y) - J_{22ij}(x,y)$$

4) A twofold integral $A_{kij}(x,y)$ is symmetrical on the transposition of i, j indexes.

$$A_{kij}(x,y) = A_{kji}(x,y)$$

5) Unknown integrals $A_{kij}(x,y)$ that contains indexes “1” or/and “2” can be obtained from the already calculated ones by simultaneous permutation of indexes “1” \leftrightarrow “2” and coordinates $x \leftrightarrow y$, e.g.: $A_{211}(x,y) \equiv A_{122}(y,x)$, $A_{213}(x,y) \equiv A_{123}(y,x)$, $A_{311}(x,y) \equiv A_{322}(y,x)$.

We derived the following expressions for original $J_{klji}(x,y)$ integrals:

$$J_{1111}(x,y) = \frac{Q}{2\pi\epsilon_0(\kappa+1)} \frac{1+\nu}{2\pi Y} \frac{\pi}{4\sqrt{d^2+\rho^2}(\sqrt{d^2+\rho^2}+d)^2 \rho^4} \times \\ \times \left(\begin{array}{l} 2d^2x^2(x^2+4y^2) + 2(d^2+\rho^2)y^2(4x^2+y^2) + \\ + d\sqrt{d^2+\rho^2}(5x^4-2x^2y^2+5y^4) + \\ + 2(1-2\nu)(2d^2x^4+2(d^2+\rho^2)y^4+d\sqrt{d^2+\rho^2}(x^4+6x^2y^2+y^4)) \end{array} \right) \quad (\text{A.6})$$

$$J_{1112}(x,y) = \frac{Q}{2\pi\epsilon_0(\kappa+1)} \frac{1+\nu}{2\pi Y} \frac{\pi x y (d x^2 + \sqrt{d^2 + \rho^2} y^2) (3 - 2(1 - 2\nu))}{2\sqrt{d^2 + \rho^2} (\sqrt{d^2 + \rho^2} + d)^3 \rho^2} \quad (\text{A.7})$$

$$J_{1122}(x,y) = \frac{Q}{2\pi\epsilon_0(\kappa+1)} \frac{1+\nu}{2\pi Y} \frac{\pi}{4\sqrt{d^2+\rho^2}(\sqrt{d^2+\rho^2}+d)^2 \rho^4} \times \\ \times \left(\begin{array}{l} 2d^2x^2(4x^2+y^2) + 2(d^2+\rho^2)y^2(x^2+4y^2) + \\ + d\sqrt{d^2+\rho^2}(5x^4+22x^2y^2+5y^4) + \\ + 2(1-2\nu)(2(2d^2+\rho^2)x^2y^2+d\sqrt{d^2+\rho^2}(x^2-y^2)^2) \end{array} \right) \quad (\text{A.8})$$

$$J_{1113}(x, y) = -\frac{Q}{2\pi\varepsilon_0(\kappa+1)} \frac{1+v}{2\pi Y} \frac{\pi x \left(2d x^2 + \sqrt{d^2 + \rho^2} (x^2 + 3y^2)\right)}{4\sqrt{d^2 + \rho^2} \left(\sqrt{d^2 + \rho^2} + d\right)^2 \rho^2} \times \\ \times (1 - 2(3 - 4 \ln 2)(1 - 2v)) \quad (\text{A.9})$$

$$J_{1123}(x, y) = -\frac{Q}{2\pi\varepsilon_0(\kappa+1)} \frac{1+v}{2\pi Y} \frac{\pi y \left(2d x^2 + \sqrt{d^2 + \rho^2} (-x^2 + y^2)\right)}{4\sqrt{d^2 + \rho^2} \left(\sqrt{d^2 + \rho^2} + d\right)^2 \rho^2} \times \\ \times (1 - 2(3 - 4 \ln 2)(1 - 2v)) \quad (\text{A.10})$$

$$J_{1133}(x, y) = \frac{Q}{2\pi\varepsilon_0(\kappa+1)} \frac{1+v}{2\pi Y} \frac{2\pi \left(d x^2 + \sqrt{d^2 + \rho^2} y^2\right)}{\sqrt{d^2 + \rho^2} \left(\sqrt{d^2 + \rho^2} + d\right) \rho^2} \times \\ \times \left(\frac{3}{4} + (3 - 4 \ln 2)(1 - 2v) \right) \quad (\text{A.11})$$

$$J_{1211}(y, x) = -\frac{Q}{2\pi\varepsilon_0(\kappa+1)} \frac{1+v}{2\pi Y} \frac{\pi x y}{\sqrt{d^2 + \rho^2} \left(\sqrt{d^2 + \rho^2} + d\right)^2} \times \\ \times \left(\begin{array}{l} d(y^2 + 4x^2) + \sqrt{d^2 + \rho^2} (4y^2 + x^2) + \\ + 2(1 - 2v)(d y^2 + \sqrt{d^2 + \rho^2} x^2) \end{array} \right) \quad (\text{A.12})$$

$$J_{1212}(x, y) = -\frac{Q}{2\pi\varepsilon_0(\kappa+1)} \frac{1+v}{2\pi Y} \frac{\pi \left(2(2d^2 + \rho^2) x^2 y^2 + d \sqrt{d^2 + \rho^2} (x^2 - y^2)^2\right)}{4\sqrt{d^2 + \rho^2} \left(\sqrt{d^2 + \rho^2} + d\right)^2 \rho^4} \times \\ \times (3 - 2(1 - 2v)) \quad (\text{A.13})$$

$$J_{1213}(x, y) = -\frac{Q}{2\pi\varepsilon_0(\kappa+1)} \frac{1+v}{2\pi Y} \frac{\pi y \left(2d x^2 + \sqrt{d^2 + \rho^2} (-x^2 + y^2)\right)}{4\sqrt{d^2 + \rho^2} \left(\sqrt{d^2 + \rho^2} + d\right)^2 \rho^2} \times \\ \times (1 - 2(3 - 4 \ln 2)(1 - 2v)) \quad (\text{A.14})$$

$$J_{1233}(x, y) = -\frac{Q}{2\pi\varepsilon_0(\kappa+1)} \frac{1+v}{2\pi Y} \frac{2\pi x y}{\sqrt{d^2 + \rho^2} \left(\sqrt{d^2 + \rho^2} + d\right)^2} \times \\ \times \left(\frac{3}{4} + (3 - 4 \ln 2)(1 - 2v) \right) \quad (\text{A.15})$$

$$J_{1311}(x, y) = -\frac{Q}{2\pi\varepsilon_0(\kappa+1)} \frac{1+v}{2\pi Y} \frac{\pi x}{4\sqrt{d^2 + \rho^2} \left(\sqrt{d^2 + \rho^2} + d\right)^2 \rho^2} \times \\ \times \left(\begin{array}{l} 2d(x^2 + 4y^2) + \sqrt{d^2 + \rho^2} (5x^2 - y^2) + \\ + 2(1 - 2v)(2d x^2 + \sqrt{d^2 + \rho^2} (x^2 + 3y^2)) \end{array} \right) \quad (\text{A.16})$$

$$J_{1312}(x, y) = \frac{Q}{2\pi\varepsilon_0(\kappa+1)} \frac{1+\nu}{2\pi Y} \frac{\pi y \left(2d x^2 + \sqrt{d^2 + \rho^2}(-x^2 + y^2)\right)}{4\sqrt{d^2 + \rho^2} \left(\sqrt{d^2 + \rho^2} + d\right)^2 \rho^2} \times \\ \times (3 - 2(1 - 2\nu)) \quad (\text{A.17})$$

$$J_{1322}(x, y) = -\frac{Q}{2\pi\varepsilon_0(\kappa+1)} \frac{1+\nu}{2\pi Y} \frac{\pi x}{4\sqrt{d^2 + \rho^2} \left(\sqrt{d^2 + \rho^2} + d\right)^2 \rho^2} \times \\ \times \left(\begin{array}{l} 2d(4x^2 + y^2) + \sqrt{d^2 + \rho^2}(5x^2 + 11y^2) + \\ + 2(1 - 2\nu)(2d y^2 + \sqrt{d^2 + \rho^2}(x^2 - y^2)) \end{array} \right) \quad (\text{A.18})$$

$$J_{1313}(x, y) = -\frac{Q}{2\pi\varepsilon_0(\kappa+1)} \frac{1+\nu}{2\pi Y} \frac{\pi \left(d x^2 + \sqrt{d^2 + \rho^2} y^2\right)}{2\sqrt{d^2 + \rho^2} \left(\sqrt{d^2 + \rho^2} + d\right) \rho^2} \times \\ \times (1 - 2(3 - 4 \ln 2)(1 - 2\nu)) \quad (\text{A.19})$$

$$J_{1323}(x, y) = \frac{Q}{2\pi\varepsilon_0(\kappa+1)} \frac{1+\nu}{2\pi Y} \frac{\pi x y}{2\sqrt{d^2 + \rho^2} \left(\sqrt{d^2 + \rho^2} + d\right)^2} \times \\ \times (1 - 2(3 - 4 \ln 2)(1 - 2\nu)) \quad (\text{A.20})$$

$$J_{1333}(x, y) = -\frac{Q}{2\pi\varepsilon_0(\kappa+1)} \frac{1+\nu}{2\pi Y} \frac{2\pi x}{\sqrt{d^2 + \rho^2} \left(\sqrt{d^2 + \rho^2} + d\right)} \times \\ \times \left(\frac{3}{4} + (3 - 4 \ln 2)(1 - 2\nu) \right) \quad (\text{A.21})$$

$$J_{3311}(x, y) = -\frac{Q}{2\pi\varepsilon_0(\kappa+1)} \frac{1+\nu}{2\pi Y} \frac{\pi}{2\sqrt{d^2 + \rho^2} \left(\sqrt{d^2 + \rho^2} + d\right)^2 \rho^2} \times \\ \times \left(\begin{array}{l} d^2(x^2 + 4y^2) + (d^2 + \rho^2)(4x^2 + y^2) + \\ + 5d\sqrt{d^2 + \rho^2}(x^2 + y^2) + \\ + 2(1 - 2\nu)(\sqrt{d^2 + \rho^2} + d)(d x^2 + \sqrt{d^2 + \rho^2} y^2) \end{array} \right) \quad (\text{A.22})$$

$$J_{3312}(x, y) = -\frac{Q}{2\pi\varepsilon_0(\kappa+1)} \frac{1+\nu}{2\pi Y} \frac{\pi x y (3 - 2(1 - 2\nu))}{2\sqrt{d^2 + \rho^2} \left(\sqrt{d^2 + \rho^2} + d\right)^2} \quad (\text{A.23})$$

$$J_{3313}(x, y) = \frac{Q}{2\pi\varepsilon_0(\kappa+1)} \frac{1+\nu}{2\pi Y} \frac{\pi x}{2\sqrt{d^2 + \rho^2} \left(\sqrt{d^2 + \rho^2} + d\right)} \times \\ \times (1 - 2(3 - 4 \ln 2)(1 - 2\nu)) \quad (\text{A.24})$$

$$J_{3333}(x, y) = -\frac{Q}{2\pi\varepsilon_0(\kappa+1)} \frac{1+\nu}{2\pi Y} \frac{2\pi}{\sqrt{d^2 + \rho^2}} \left(\frac{3}{4} + (3 - 4 \ln 2)(1 - 2\nu) \right) \quad (\text{A.25})$$

The original integrals $A_{ijk}(x, y)$ have the following form:

$$A_{111}(x, y) = \frac{Q}{2\pi\varepsilon_0(\kappa+1)} \frac{1+\nu}{2\pi Y} \frac{\pi x}{\sqrt{d^2 + \rho^2} \left(\sqrt{d^2 + \rho^2} + d \right)^2 \rho^2} \times \\ \times \left(\begin{array}{l} \sqrt{d^2 + \rho^2} (3x^2 + y^2) + 2d(x^2 + 2y^2) + \\ + (1-2\nu) \left(\sqrt{d^2 + \rho^2} (x^2 + 3y^2) + 2d x^2 \right) \end{array} \right) \quad (\text{A.26})$$

$$A_{112}(x, y) = -\frac{Q}{2\pi\varepsilon_0(\kappa+1)} \frac{1+\nu}{2\pi Y} \frac{\pi y \left(\sqrt{d^2 + \rho^2} (-x^2 + y^2) + 2d x^2 \right)}{\sqrt{d^2 + \rho^2} \left(\sqrt{d^2 + \rho^2} + d \right)^2 \rho^2} (1 - (1-2\nu)) \quad (\text{A.27})$$

$$A_{113}(x, y) \equiv 0 \quad (\text{A.28})$$

$$A_{122}(x, y) = \frac{Q}{2\pi\varepsilon_0(\kappa+1)} \frac{1+\nu}{2\pi Y} \frac{\pi x}{\sqrt{d^2 + \rho^2} \left(\sqrt{d^2 + \rho^2} + d \right)^2 \rho^2} \times \\ \times \left(\begin{array}{l} \sqrt{d^2 + \rho^2} (3x^2 + 5y^2) + 2d(2x^2 + y^2) + \\ + (1-2\nu) \left(\sqrt{d^2 + \rho^2} (x^2 - y^2) + 2d y^2 \right) \end{array} \right) \quad (\text{A.29})$$

$$A_{123}(x, y) \equiv 0 \quad (\text{A.30})$$

$$A_{133}(x, y) = -\frac{Q}{2\pi\varepsilon_0(\kappa+1)} \frac{1+\nu}{2\pi Y} \frac{2\pi x}{\sqrt{d^2 + \rho^2} \left(\sqrt{d^2 + \rho^2} + d \right)} (1 + (1-2\nu)) \quad (\text{A.31})$$

$$A_{311}(x, y) = \frac{Q}{2\pi\varepsilon_0(\kappa+1)} \frac{1+\nu}{2\pi Y} \frac{2\pi}{\sqrt{d^2 + \rho^2} \left(\sqrt{d^2 + \rho^2} + d \right) \rho^2} \times \\ \times \left(\begin{array}{l} \sqrt{d^2 + \rho^2} (2x^2 + y^2) + d(x^2 + 2y^2) + \\ + (1-2\nu) \left(\sqrt{d^2 + \rho^2} y^2 + d x^2 \right) \end{array} \right) \quad (\text{A.32})$$

$$A_{312}(x, y) = \frac{Q}{2\pi\varepsilon_0(\kappa+1)} \frac{1+\nu}{2\pi Y} \frac{2\pi x y (1 - (1-2\nu))}{\sqrt{d^2 + \rho^2} \left(\sqrt{d^2 + \rho^2} + d \right)^2} \quad (\text{A.33})$$

$$A_{313}(x, y) \equiv 0 \quad (\text{A.34})$$

$$A_{333}(x, y) = \frac{Q}{2\pi\varepsilon_0(\kappa+1)} \frac{1+\nu}{2\pi Y} \frac{2\pi}{\sqrt{d^2 + \rho^2}} (1 + (1-2\nu)) \quad (\text{A.35})$$

For further consideration we need to calculate the components $U_{klj}(x=0, y=0) = -J_{klj}(0,0) - \delta_{l3} A_{kij}(0,0)$ ($z=0$).

It is appeared that tensor U_{klj} is symmetrical on the transposition of the indexes i, j and k, l . This allows one to use the Voigt matrix notations for $U_{klj}(0)$:

$$\begin{aligned} U_{1111}(0,0) &\equiv U_{11}, & U_{2222}(0,0) &\equiv U_{22}, & U_{3333}(0,0) &\equiv U_{33} \\ U_{2323}(0,0) &\equiv U_{44}, & U_{1313}(0,0) &\equiv U_{55}, & U_{1212}(0,0) &\equiv U_{66} \end{aligned} \quad (\text{A.36})$$

$$U_{1122}(0,0) \equiv U_{12}, \quad U_{2211}(0,0) \equiv U_{21}, \quad U_{1133}(0,0) \equiv U_{13}, \quad U_{3311}(0,0) \equiv U_{31}$$

The tensor $\hat{U}(0)$ in matrix form has the view:

$$\hat{U}(0) = \frac{Q}{2\pi\epsilon_0(\kappa+1)} \frac{1+v}{Y} \frac{1}{d} \begin{pmatrix} a_{11} & a_{12} & a_{13} & 0 & 0 & 0 \\ a_{12} & a_{11} & a_{13} & 0 & 0 & 0 \\ a_{31} & a_{31} & a_{33} & 0 & 0 & 0 \\ 0 & 0 & 0 & a_{44} & 0 & 0 \\ 0 & 0 & 0 & 0 & a_{44} & 0 \\ 0 & 0 & 0 & 0 & 0 & a_{66} \end{pmatrix} \quad (\text{A.37})$$

Here the following designation is introduced:

$$\begin{aligned} a_{11} &\equiv -\frac{7+6(1-2v)}{32}, & a_{12} &\equiv -\frac{13+2(1-2v)}{32}, \\ a_{13} &\equiv -\frac{3}{8} - \frac{3-4\ln 2}{2}(1-2v), & a_{31} &\equiv -\frac{7+2(1-2v)}{8}, \\ a_{33} &\equiv -\frac{1}{4} + (2-4\ln 2)(1-2v), \\ a_{44} &\equiv \frac{1}{8} - \left(\frac{3}{4} - \ln 2\right)(1-2v), & a_{66} &\equiv \frac{3-2(1-2v)}{32}, \end{aligned} \quad (\text{A.38})$$

APPENDIX B. Integration method

When integrating (A.3) and (A.4) at $x_3 = 0$ we introduce new coordinate system $\tilde{x} = x'_1 - x_1$, $\tilde{y} = x'_2 - x_2$ and used the designations $x_1 \equiv x$, $x_2 \equiv y$. Then in Eq. (A.3) we turn to the spherical coordinates $\tilde{x} = r \sin(\theta) \cos(\varphi)$, $\tilde{y} = r \sin(\theta) \sin(\varphi)$, $x'_3 = r \cos(\theta)$, where φ is vectorial (polar) angle and θ is angle of elevation. Therefore Green's function will depend on the angles only $G_{ij}(\tilde{x}, \tilde{y}, x'_3, x_3 = 0) \equiv G_{ij}(\sin(\theta) \cos(\varphi), \sin(\theta) \sin(\varphi), \cos(\theta), 0) / r$. The field gradients $\partial E_k(\tilde{x} + x, \tilde{y} + y, x'_3) / \partial x'_i$ contain nontrivial dependence on r, x, y and angles θ, φ .

The integration on polar radius r is reduced to four similar quadratures:

$$\int_0^\infty \frac{r dr}{(r^2 + 2pr + a^2)^{3/2}} = \frac{1}{a+p}, \quad \int_0^\infty \frac{3r dr}{(r^2 + 2pr + a^2)^{5/2}} = \frac{1}{a(a+p)^2} \quad (\text{B.1})$$

$$\int_0^\infty \frac{3r^2 dr}{(r^2 + 2pr + a^2)^{5/2}} = \frac{1}{(a+p)^2}, \quad \int_0^\infty \frac{3r^3 dr}{(r^2 + 2pr + a^2)^{5/2}} = \frac{a}{(a+p)^2} + \frac{1}{a+p} \quad (\text{B.2})$$

The integrals (B.1), (B.2) are taken under conditions $a > 0$, $a^2 > p^2$ that is indeed true since $a^2 \equiv d^2 + x^2 + y^2$, $p \equiv x \sin(\theta) \cos(\varphi) + y \sin(\theta) \sin(\varphi) + d \cos(\theta)$.

The integration on polar angle φ reduces to the following integrals

$$\int_0^{2\pi} \frac{d\varphi}{\alpha + \beta \cos(\varphi) + \chi \sin(\varphi)} = \frac{2\pi}{\sqrt{\alpha^2 - \beta^2 - \chi^2}} \quad (B.3)$$

$$\int_0^{2\pi} \frac{\cos(\varphi) d\varphi}{\alpha + \beta \cos(\varphi) + \chi \sin(\varphi)} = -\frac{2\pi\beta}{\sqrt{\alpha^2 - \beta^2 - \chi^2}} \frac{1}{\sqrt{\alpha^2 - \beta^2 - \chi^2} + \alpha} \quad (B.4)$$

$$\int_0^{2\pi} \frac{\sin(\varphi) d\varphi}{\alpha + \beta \cos(\varphi) + \chi \sin(\varphi)} = -\frac{2\pi\chi}{\sqrt{\alpha^2 - \beta^2 - \chi^2}} \frac{1}{\sqrt{\alpha^2 - \beta^2 - \chi^2} + \alpha} \quad (B.5)$$

$$\int_0^{2\pi} \frac{\cos(\varphi)^2 d\varphi}{\alpha + \beta \cos(\varphi) + \chi \sin(\varphi)} = \frac{2\pi}{(\beta^2 + \chi^2)^2} \left(-\alpha(\beta^2 - \chi^2) + \frac{\alpha^2(\beta^2 - \chi^2) + \chi^2(\beta^2 + \chi^2)}{\sqrt{\alpha^2 - \beta^2 - \chi^2}} \right) \quad (B.6)$$

$$\int_0^{2\pi} \frac{\sin(\varphi)^2 d\varphi}{\alpha + \beta \cos(\varphi) + \chi \sin(\varphi)} = \frac{2\pi}{(\beta^2 + \chi^2)^2} \left(\alpha(\beta^2 - \chi^2) + \frac{-\alpha^2(\beta^2 - \chi^2) + \beta^2(\beta^2 + \chi^2)}{\sqrt{\alpha^2 - \beta^2 - \chi^2}} \right) \quad (B.7)$$

$$\int_0^{2\pi} \frac{\cos(\varphi) \sin(\varphi) d\varphi}{\alpha + \beta \cos(\varphi) + \chi \sin(\varphi)} = \frac{2\pi\beta\chi}{2\alpha(\alpha^2 - \beta^2 - \chi^2) + (2\alpha^2 - \beta^2 - \chi^2)\sqrt{\alpha^2 - \beta^2 - \chi^2}} \quad (B.8)$$

$$\begin{aligned} & \int_0^{2\pi} \frac{\sin(\varphi)^3 d\varphi}{\alpha + \beta \cos(\varphi) + \chi \sin(\varphi)} = \\ &= \frac{2\pi\chi}{(\beta^2 + \chi^2)^3} \left(-2\alpha^2(3\beta^2 - \chi^2) + (3\beta^2 + \chi^2)(\beta^2 + \chi^2) + \frac{\alpha^3(6\beta^2 - 2\chi^2) - 6\alpha\beta^2(\beta^2 + \chi^2)}{\sqrt{\alpha^2 - \beta^2 - \chi^2}} \right) \quad (B.9) \end{aligned}$$

$$\begin{aligned} & \int_0^{2\pi} \frac{\cos(\varphi)^3 d\varphi}{\alpha + \beta \cos(\varphi) + \chi \sin(\varphi)} = \\ &= \frac{2\pi\beta}{(\beta^2 + \chi^2)^3} \left(2\alpha^2(\beta^2 - 3\chi^2) + (\beta^2 + 3\chi^2)(\beta^2 + \chi^2) + \frac{-\alpha^3(2\beta^2 - 6\chi^2) - 6\alpha\chi^2(\beta^2 + \chi^2)}{\sqrt{\alpha^2 - \beta^2 - \chi^2}} \right) \quad (B.10) \end{aligned}$$

Similar integrals $\int_0^{2\pi} d\varphi \cos(\varphi)^n \sin(\varphi)^m / (\alpha + \beta \cos(\varphi) + \chi \sin(\varphi))^2$ can be found by the differentiation of (B.3)-(B.10) on parameters α, β, χ . It should be noted that (B.3)-(B.10) are taken under conditions $\alpha > 0$, $\alpha^2 > \beta^2 + \chi^2$ that is indeed true since $\alpha \equiv \sqrt{d^2 + x^2 + y^2} + d \cos(\theta)$, $\beta \equiv x \sin(\theta)$, $\chi \equiv y \sin(\theta)$.

When integrating on θ we turn to new variable $t = \cos(\theta)$. It is appeared that integrands are reduced to rational functions on t . These simple but rather lengthy calculation led to the analytical expressions for $J_{klj}(x, y)$ and $A_{klj}(x, y)$.

References

¹ P. GÜTHNER and K. DRANSFELD, *Appl. Phys. Lett.* **61**, 1137 (1992).

² *Nanoscale Characterization of Ferroelectric Materials*, ed. M. Alexe and A. Gruverman, Springer (2004).

³ *Nanoscale Phenomena in Ferroelectric Thin Films*, ed. S. Hong, Kluwer (2004).

⁴ C. Harnagea, A. Pignolet, M. Alexe, D. Hesse, and U. Gösele, *Appl. Phys. A* **70**, 261 (2000).

⁵ B. J. Rodriguez, A. Gruverman, A.I. Kingon, R.J. Nemanich, and J.S. Cross, *J. Appl. Phys.* **95**, 1958 (2004).

⁶ S.V. Kalinin, E. Karapetian, and M. Kachanov, *Phys. Rev. B* **70**, 184101 (2004).

⁷ E. Karapetian, M. Kachanov, and S.V. Kalinin, *Phil. Mag.* **85**, 1017 (2005).

⁸ C.S. Ganpule, V. Nagarjan, H. Li, A.S. Ogale, D.E. Steinhauer, S. Aggarwal, E. Williams, R. Ramesh, and P. De Wolf, *Appl. Phys. Lett.* **77**, 292 (2000).

⁹ A. Agronin, M. Molotskii, Y. Rosenwaks, E. Strassburg, A. Boag, S. Mutchnik, and G. Rosenman, *J. Appl. Phys.* **97**, 084312 (2005)

¹⁰ F. Felten, G. A. Schneider, J. Muñoz Saldaña, and S. V. Kalinin, *J. Appl. Phys.* **96**, 563 (2004).

¹¹ D.A. Scrymgeour and V. Gopalan, *Phys. Rev. B* **72**, 024103 (2005).

¹² R.E. Newnham, *Properties of Materials: Anisotropy, Symmetry, Structure*, New York, Oxford University Press, 2005.

¹³ S.V. Kalinin and D.A. Bonnell, *Phys. Rev. B* **65**, 125408 (2002).

¹⁴ S. Belaidi, P. Girard, and G. Leveque, *J. Appl. Phys.* **81**, 1023 (1997).

¹⁵ T. Mura, *Micromechanics of Defects in Solids*, Martinus Nijhoff, Dordrecht, 1987.

¹⁶ L.M. Eng, H.-J. Guntherodt, G.A. Schneider, U.Kopke, and J.M. Saldana, *Appl. Phys. Lett.* **74**, 233 (1999).

¹⁷ S.V. Kalinin, B.J. Rodriguez, S. Jesse, J. Shin, A.P. Baddorf, P. Gupta, H. Jain, D.B. Williams, and A. Gruverman, *Microscopy and Microanalysis*, in print

¹⁸ Note that the full form has to be used in final calculations

¹⁹ E.A. Eliseev, S.V. Kalinin, and A.N. Morozovska, to be submitted